Research Article | Vol. 24, No. 16 | 8 Aug 2016 | OPTICS EXPRESS 17728

Optics EXPRESS

Surface plasmon optical antennae in the infrared region with high resonant efficiency and frequency selectivity

KOSEI UENO,[1,*] QUAN SUN,[1] MASAHIRO MINO,[1] TAKUMI ITOH,[1] TOMOYA OSHIKIRI,[1] AND HIROAKI MISAWA[1,2]

[1] *Research Institute for Electronic Science, Hokkaido University, N21, W10, Kita-ku, 001-0021, Sapporo, Japan*

[2] *Department of Applied Chemistry & Institute of Molecular Science, National Chiao Tung University, 1001 Ta Hsueh R., Hsinchu 30010, Taiwan*

[*] *k-ueno@es.hokudai.ac.jp*

Abstract: Infrared light has received attention for sensor applications, including fingerprint spectroscopy, in the bioengineering and security fields. Surface plasmon physics enables the operation of a light harvesting optical antenna. Gold nanochains exhibit localized surface plasmon resonance (LSPR) in the infrared region with high frequency selectivity. However, a feasible design for optical antennae with a higher resonant efficiency and frequency selectivity as a function of structural design and periodicity is still unknown. In the present study, we investigated the relationship between the resonant efficiency and frequency selectivity as a function of the structural design of gold nanochains and explored structural periodicity for obtaining highly frequency-selective optical antennae. An optical antenna design with higher resonant efficiency is proposed on the basis of its efficient interaction with non-polarized light.

©2016 Optical Society of America

OCIS codes: (240.6680) Surface plasmons; (250.5403) Plasmonics.

References and links

1. J. F. Federici, B. Schulkin, F. Huang, D. Gary, R. Barat, F. Oliveira, and D. Zimdars, "THz imaging and sensing for security applications-explosives, weapons and drugs," J. Semicond. Tech. Sci. **20**(7), S266–S280 (2005).
2. M. Tonouchi, "Cutting-edge terahertz technology," Nat. Photonics **1**(2), 97–105 (2007).
3. R. Piesiewicz, T. Kleine-Ostmann, N. Krumbholz, D. Mittleman, M. Koch, J. Schoebei, and T. Kurner, "Short-range ultra-broadband terahertz communications: concepts and perspectives," IEEE Antennas Propagation **49**(6), 24–39 (2007).
4. Z. Fang, Z. Liu, Y. Wang, P. M. Ajayan, P. Nordlander, and N. J. Halas, "Graphene-antenna sandwich photodetector," Nano Lett. **12**(7), 3808–3813 (2012).
5. Y. Yao, M. A. Kats, P. Genevet, N. Yu, Y. Song, J. Kong, and F. Capasso, "Broad electrical tuning of graphene-loaded plasmonic antennas," Nano Lett. **13**(3), 1257–1264 (2013).
6. A. Shalabney, J. George, J. Hutchison, G. Pupillo, C. Genet, and T. W. Ebbesen, "Coherent coupling of molecular resonators with a microcavity mode," Nat. Commun. **6**, 5981 (2015).
7. A. Toma, S. Tuccio, M. Prato, F. De Donato, A. Perucchi, P. Di Pietro, S. Marras, C. Liberale, R. Proietti Zaccaria, F. De Angelis, L. Manna, S. Lupi, E. Di Fabrizio, and L. Razzari, "Squeezing terahertz light into nanovolumes: nanoantenna enhanced terahertz spectroscopy (NETS) of semiconductor quantum dots," Nano Lett. **15**(1), 386–391 (2015).
8. A. Ishikawa and T. Tanaka, "Metamaterial absorbers for infrared detection of molecular self-assembled monolayers," Sci. Rep. **5**, 12570 (2015).
9. K. Ueno, S. Nozawa, and H. Misawa, "Surface-enhanced terahertz spectroscopy using gold rod structures resonant with terahertz waves," Opt. Express **23**(22), 28584–28592 (2015).
10. S. Link and M. A. El-Sayed, "Spectral properties and relaxation dynamics of surface plasmon electronic oscillations in gold and silver nanodots and nanorods," J. Phys. Chem. B **103**(40), 8410–8426 (1999).
11. K. L. Kelly, E. Coronado, L. L. Zhao, and G. C. Schatz, "The optical properties of metal nanoparticles: The influence of size, shape, and dielectric environment," J. Phys. Chem. B **107**(3), 668–677 (2003).
12. Y.-Y. Yu, S.-S. Chang, C.-L. Lee, and C. R. C. Wang, "Gold nanorods: electrochemical synthesis and optical properties," J. Phys. Chem. B **101**(34), 6661–6664 (1997).
13. F. Kim, J. H. Song, and P. Yang, "Photochemical synthesis of gold nanorods," J. Am. Chem. Soc. **124**(48), 14316–14317 (2002).

#267247 http://dx.doi.org/10.1364/OE.24.017728
Journal © 2016 Received 27 May 2016; revised 22 Jul 2016; accepted 22 Jul 2016; published 26 Jul 2016

Optics EXPRESS

14. L. Razzari, A. Toma, M. Clerici, M. Shalaby, G. Das, C. Liberale, M. Chirumamilla, R. P. Zaccaria, F. De Angelis, M. Peccianti, R. Morandotti, and E. Di Fabrizio, "Terahertz dipole nanoantenna arrays: resonance characteristics," Plasmonics **8**(1), 133–138 (2013).
15. K. Ueno, S. Juodkazis, V. Mizeikis, D. Ohnishi, K. Sasaki, and H. Misawa, "Inhibition of multipolar plasmon excitation in periodic chains of gold nanoblocks," Opt. Express **15**(25), 16527–16539 (2007).
16. F. Wen, Y. Zhang, S. Gottheim, N. S. King, Y. Zhang, P. Nordlander, and N. J. Halas, "Charge transfer plasmons: optical frequency conductances and tunable infrared resonances," ACS Nano **9**(6), 6428–6435 (2015).
17. K. Ueno and H. Misawa, "Spectral properties and electromagnetic field enhancement effects on nano-engineered metallic nanoparticles," Phys. Chem. Chem. Phys. **15**(12), 4093–4099 (2013).
18. X. Wang, P. Gogol, E. Cambril, and B. Palpant, "Near- and far-field effects on the plasmon coupling in gold nanoparticle arrays," J. Phys. Chem. C **116**(46), 24741–24747 (2012).
19. A. C. Lesina, A. Vaccari, P. Berini, and L. Ramunno, "On the convergence and accuracy of the FDTD method for nanoplasmonics," Opt. Express **23**(8), 10481–10497 (2015).
20. K. Imura, K. Ueno, H. Misawa, H. Okamoto, D. McArthur, B. Hourahine, and F. Papoff, "Plasmon modes in single gold nanodiscs," Opt. Express **22**(10), 12189–12199 (2014).

1. Introduction

Infrared light has received considerable attention for use in many applications such as high speed communications, transmission imaging and fingerprint spectra with important roles in the bioengineering and security fields [1–3]. An optical antenna design is desired with high resonant efficiency and frequency selectivity in the infrared region. Surface plasmons are expected to play a role in the light harvesting optical antenna in the wavelength region [4,5]. In particular, it has been recently proposed that a small number of molecules can be detected using spectral modulation induced by an interaction between the molecular/intermolecular vibrational mode and surface plasmons in the infrared wavelength region [6–9]. Therefore, a viable design for plasmonic antennae in the frequency region would enable improved sensitivity.

Nanoparticles of noble metal such as gold exhibit very intense color, which is derived from localized surface plasmon resonance (LSPR) [10,11]. To induce LSPR in the near-infrared, a gold nanorod with a relatively long length has been synthesized according to the reduction of chloroauric acid using cylindrical surfactant micelles as a template [12,13]. Furthermore, the LSPR wavelength of optical antennae responds to the far-infrared region when the rod length is lengthened from approximately 1 μm to 10 μm with a higher aspect ratio as defined by the ratio of length to width [7,9,14]. An optical antenna structure has also been designed that responds to the mid-infrared region by increasing the length by linking many gold nanoblocks using nanofabrication techniques rather than lengthening a single rod [15]; this design enables the creation of charge transfer plasmons [16]. These studies focused on developing structures to exhibit plasmon resonance in the infrared region and did not specifically address the design of optical antennae with high resonant efficiency and frequency selectivity.

A high resonant efficiency and frequency selectivity is not necessarily obtained even if the rod length is increased and the rods are arranged regularly in order. Higher-order plasmon modes are excited because the total volume of the rod increases with rod length, and therefore several modes such as the hexapole mode are induced in the higher-frequency region compared to the dipole mode. As a result, the frequency selectivity decreases because new peaks appear in the higher-frequency region compared to the dipole mode. To overcome this problem, we previously proposed a gold nanochain in which several gold nanoblocks are regularly and diagonally aligned with a link [15]. Gold nanochains offer the feature that higher-order modes cannot be induced easily because the apparent aspect ratio increases as a result of the narrow bottleneck width [15]. However, the resonant efficiency also decreases because plasmon damping is induced by a resistivity based on the narrow bottleneck between nanoblocks. If the nanoblocks are separated with a small nanogap, LSPR does not exist in mid- and far-infrared regions although few spectrum shifts to the longer wavelength can be seen due to the dipole-dipole interaction between the nanoblocks [17].

To increase the resonant efficiency, it is not necessary to reduce the pitch of periodic structures. Careful design of periodic structures enables both near-field interactions between

Optics EXPRESS

rods or chains and the influence of far-field coupling [18]. Furthermore, the extinction spectrum becomes broader because linear polarized light along the transverse direction cannot be transmitted to the substrate by diffraction if the structural periodicity along the transverse direction is smaller because the periodic structure works as a linear polarizer. In the present study, we focus on a structural design for obtaining gold nanochains with a high resonant efficiency and frequency selectivity. Here, the resonant efficiency and frequency selectivity are defined as the extinction value and the peak ratio between the fundamental plasmon mode and the other modes such as higher order plasmon resonances, respectively. First, we explore the relationship between the resonant efficiency and frequency selectivity as a function of the structural design of gold nanochains. In particular, the importance of the bottleneck width is discussed. Second, we elucidate structural periodicity for highly frequency-selective optical antennae. Finally, we explore the design of optical antennae with higher resonant efficiency from the viewpoint of efficient interaction with non-polarized light.

2. Experimental

Ordered arrays of gold nanochains were fabricated on a silicon or a sapphire substrate using electron beam lithography and lift-off techniques [17]. After washing the substrate with acetone, methanol, and pure water, a positive resist film used in electron beam lithography (ZEP520a, Zeon Chemicals Co.) was deposited by spin-coating to a thickness of 200 nm on the substrate. The resist film was then exposed to the desired pattern using an electron beam lithography system (ELS-7000, Elionix Co.) with an accelerating voltage of 100 kV. Then, the exposed resist film was developed and rinsed with a developer solution (Anisole, Wako Pure Chemical Industries, Ltd.) and a rinsing agent (ZMD-B, Zeon Chemicals Co.). Chromium and gold thin films were deposited by sputtering onto the developed substrate (MPS-4000C1/HC1, ULVAC Co.), and a lift-off process was conducted with a resist remover solution (ZDMAC, Zeon Chemicals Co.), resulting in the formation of gold nanochains on the substrate. The extinction spectrum in the infrared wavelength region was measured by a Fourier transform infrared (FT-IR-6000TM-M) spectrometer equipped with a microscope attachment (FT-IR, IRT-3000, Jasco Co.). In the frequency region lower than 667 cm^{-1}, FT-IR for the far infrared region (FT/IR-6300FV, Jasco Co.) was employed. The area patterned by electron beam exposure was 50 μm × 50 μm for the extinction spectrum measurement in the frequency region higher than 667 cm^{-1} (20 THz) and 5 mm × 5 mm for the frequency region lower than 667 cm^{-1} (20 THz). The FDTD Solutions software package (Lumerical, Inc.) was used to numerically calculate the extinction spectrum of gold nanochains. The sapphire and silicon substrates were assumed to behave as a dielectric with an average refractive index of n = 1.76 and 3.42, respectively. The FDTD simulations were performed on a discrete, nonuniformly spaced mesh with a maximum resolution of 3 nm [19]. In the plane of the substrate surface (x-y), we use periodic boundary conditions. In the light propagation direction (z), perfectly-matched layer (PML) boundary conditions were imposed at the boundaries of the calculation domain, which was chosen large enough to avoid truncation of the field [15]. Extinction spectrum in the FDTD simulation was obtained by the following equation:

$$\text{Extinction} = -\log T \tag{1}$$

where T is transmittance.

3. Results and discussion

3.1 Frequency selectivity of plasmon resonance band responding to a bottleneck width

To control the bottleneck width of gold nanochains while keeping the total length of the nanochain at a constant value, we designed four nanostructure shapes to populate a gold nanochain, as shown in Fig. 1(a), which shows a top view of square, circular, triangular, and rhomboid shapes. The thickness of each nanochain was designed to be 30 nm. Figure 1(a)

Optics EXPRESS

shows a schematic illustration of the designed gold nanochains; those five gold nanostructures are diagonally aligned, and each nanostructure is overlapped 30 nm to maintain a total length of 655 nm with four bottlenecks between nanostructures. We emphasize that the bottleneck width can be controlled by changing the shape of the nanostructures. The designed bottleneck width differs in each nanostructure: 30 nm for the square, 90 nm for the circle, 60 nm for the triangle and 60 nm for the rhombus. Scanning electron microscope (SEM) images of gold nanochains with different shapes of gold nanostructures fabricated on a sapphire substrate are shown in Figs. 1(b)-1(e). The gold nanochains were successfully fabricated nearly as designed, although the average bottleneck width of the circle was 88 nm and that of the triangle and rhombus was 67 nm. The bottleneck width and the structural size had a size distribution with a standard deviation of approximately 3 nm, and the corner of the nanostructures was rounded with a curvature radius of approximately 16 nm in the case of the square nanostructure.

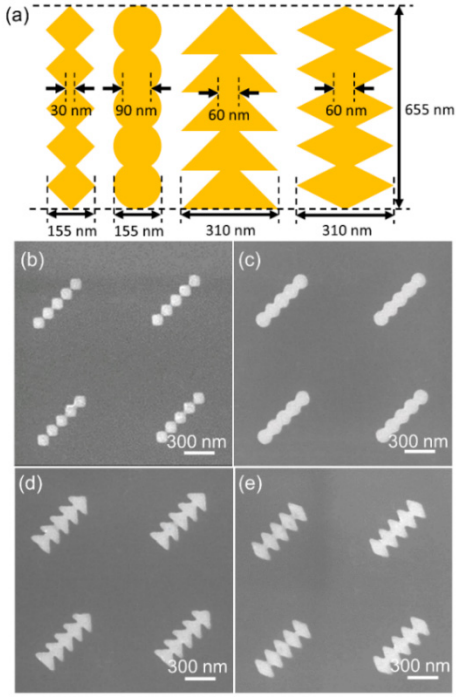

Fig. 1. (a) Schematic illustration of the designed gold nanochains composed of nanostructures; the top view of the square, triangular, rhomboid, and disk shapes are shown. Inset dimensions show the side length or diameter of the circle, the total length, and the bottleneck width. SEM images of gold nanochains consisting of five squares (b), circles (c), triangles (d), and rhombuses (e). The thickness of the gold nanochains was set at 30 nm.

Figures 2(a) and 2(b) show extinction spectra of gold nanochains consisting of square and circular nanostructures, respectively. The spectra of gold nanochains with a different chain length were measured under non-polarized conditions, and the chain length was controlled by the number of nanostructures composing a gold nanochain. Each spectrum exhibits two distinct peaks. One is approximately 13,000 cm^{-1} in square nanostructures and 12000 cm^{-1} in circular nanostructures, and the peak wavenumber is nearly independent of chain length. In contrast, the other peak with a lower wavenumber exhibits a monotonic lower frequency shift with increasing chain length. From a separate spectral measurement under linearly polarized conditions, it was determined that the peak with a relatively higher wavenumber originates from dipole plasmon resonance in the transverse mode (T-mode, the plasmon mode perpendicular to the chain), and the peak with a relatively lower wavenumber originates from

Optics EXPRESS

dipole plasmon resonance in the longitudinal mode (L-mode, the plasmon mode parallel to the chain). Therefore, only the L-mode peak exhibited a spectral shift with increasing chain length.

Notably, the peak wavenumber, extinction value and spectral width differ between square and circular nanostructures. Figure 2(c) shows the chain length dependence of the L-mode peak wavelength with gold nanochains composed of square, circular, triangular, and rhomboid nanostructures. The L-mode peak wavelength linear increases with chain length for each gold nanochain. It was observed that the L-mode peak wavelength of gold nanochains composed of square nanostructures was the longest when the chain length was the same and that the peak wavelength was nearly the same in the nanochains consisting of triangular and rhomboid nanostructures. In particular, the L-mode peak wavelength was highly dependent on the chain length as well as the bottleneck width, and the peak wavelength was longer in the gold nanochains with narrower bottleneck width.

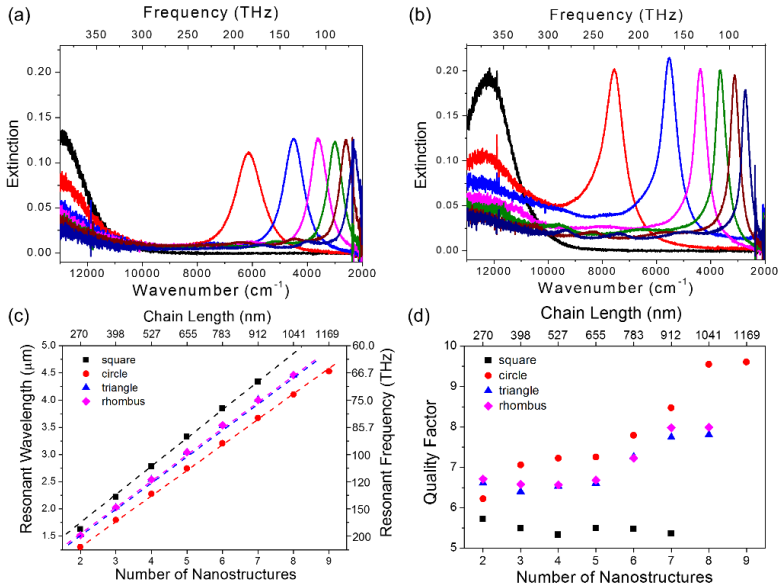

Fig. 2. Extinction spectra of gold nanochains consisting of square (a) and circular nanostructures (b) with a different chain length; 270 nm red line, 398 nm blue line, 527 nm pink line, 655 nm green line, 783 nm brown line, and 912 nm navy line. The black line is extinction spectrum of one square (a) and circular (b) nanostructures, respectively. (c) Chain length dependence of the L-mode peak wavelength with gold nanochains consisting of square, circular, triangular, and rhomboid nanostructures. (d) The quality factor as a function of the chain length of gold nanochains consisting of square, circular, triangular, and rhomboid nanostructures.

Figure 2(d) shows the quality factor as a function of the chain length of gold nanochains consisting of square, circular, triangular, and rhomboid nanostructures. The quality factor is defined as the resonant frequency divided by its spectrum width based on the full width at half maximum of the spectrum [15]. The quality factor of circular nanostructures is the highest because the spectrum width is relatively sharper. In addition, the quality factor is nearly the same in the nanochains consisting of triangular and rhomboid nanostructures because the resonant frequency and its spectrum width are identical each other. Namely, the spectral width is narrower in the gold nanochains with a broader bottleneck width because the narrower bottleneck induces damping as a result of the low conductivity between nanostructures.

Finite-difference time-domain (FDTD) simulations were performed to confirm the spectral properties of gold nanochains. Figures 3(a) and 3(b) compare experimental and simulated extinction spectra of gold nanochains consisting of square and circular nanostructures. The FDTD extinction spectra were obtained using linear polarized light along the chain. Peak positions of the simulated extinction spectra were similar to those of the experimental

Optics EXPRESS

extinction spectra, respectively. It is noteworthy that small peaks around 7200 cm^{-1} in square nanostructures and 9800 cm^{-1} in circular nanostructures can be seen in the simulated spectra. The inset figures in Figs. 3(a) and 3(b) show a near-field intensity distribution of each peak. The small peaks can be assigned as a hexapole mode from the near-field intensity distribution in Figs. 3(a) and 3(b) and the charge distribution (data were not shown here), which is induced by a far-field coupling based on the periodic array of nanochains. Importantly, the hexapole peak of circular nanostructures is relatively larger in experimental and simulated spectra as shown in Fig. 3(b). Namely, the gold nanochains with narrower bottlenecks exhibit better frequency selectivity, which corresponds to a higher peak ratio between dipole and hexapole modes, although the extinction values are low, which constitutes a trade-off. However, it is necessary to use gold nanochains with square nanostructures for the purpose of higher frequency selectivity.

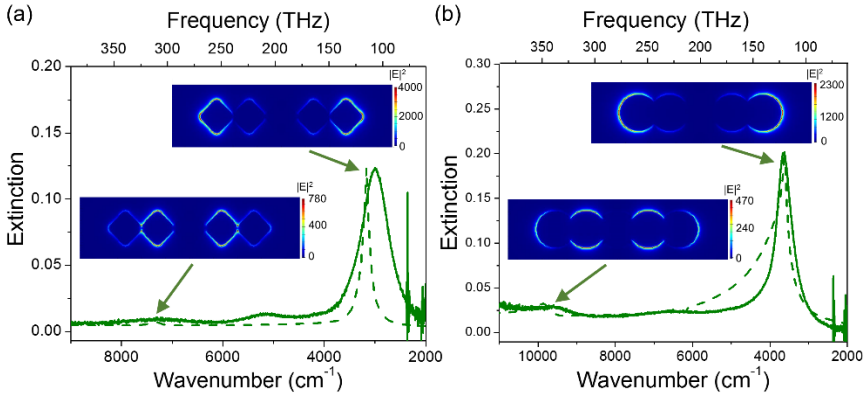

Fig. 3. The experimental and the simulated extinction spectra of gold nanochains containing five square (a) and circular (b) nanostructures with a chain length of 655 nm. The inset figures show a near-field intensity distribution of each peak. The experimental extinction spectra were taken from Figs. 2(a) and 2(b).

3.2 Frequency selectivity in plasmon resonance originating from structural periodicity

To elucidate the effect of structural periodicity on the resonant efficiency and the frequency selectivity of plasmon resonance in the infrared region, we designed an ordered array of gold nanochains with square nanostructures as shown in Fig. 4(a). Here, a is the structural periodicity and b is the chain length. Spectral properties were studied as a function of two parameters: one is the structural periodicity relative to the chain length (a/b) from 1.25 to 2.25, and the other is a rotating angle (θ) relative to the transverse axis from 0 to 60°. For example, the distance between the nearest nanochains becomes about 1.1, 1.2, 1.3, and 1.5 times longer than that with θ of 0 when the structures (a/b: 2) are rotated with θ of 15°, 30°, 45° and 60°, respectively. The extinction value and the peak ratio between dipole and hexapole modes were employed for the evaluation of the resonant efficiency and frequency selectivity in this study. Figures 4(b) and 4(c) show typical SEM images of gold nanochains containing between ten and thirty square nanostructures (a/b = 2) with θ of 0 and 60°, respectively. The thickness of each nanochain was 30 nm. In this study, a silicon substrate that transmits infrared light with a wide spectral range was used because the spectral properties in the far infrared region were also of interest. Figure 4(d) depicts extinction spectra of gold nanochains composed of ten square nanostructures with various structural periodicity values (a/b: 1.25, 1.5, 1.75, 2, and 2.25). The rotating angle θ was set at 0 as shown in the SEM image of Fig. 4(b). When the structural periodicity ratio was set relatively larger such as 2.25 or 2, a dipole plasmon resonance band of approximately 1050 cm^{-1} was clearly detected. In the spectrum, the noisy feature at approximately 2380 cm^{-1} and the small dip at approximately 1260 cm^{-1} originate from the absorption of carbon dioxide in the atmosphere and from spectral modulation influenced by the Si-O-Si asymmetric stretching vibrational mode on the silicon surface.

Optics EXPRESS

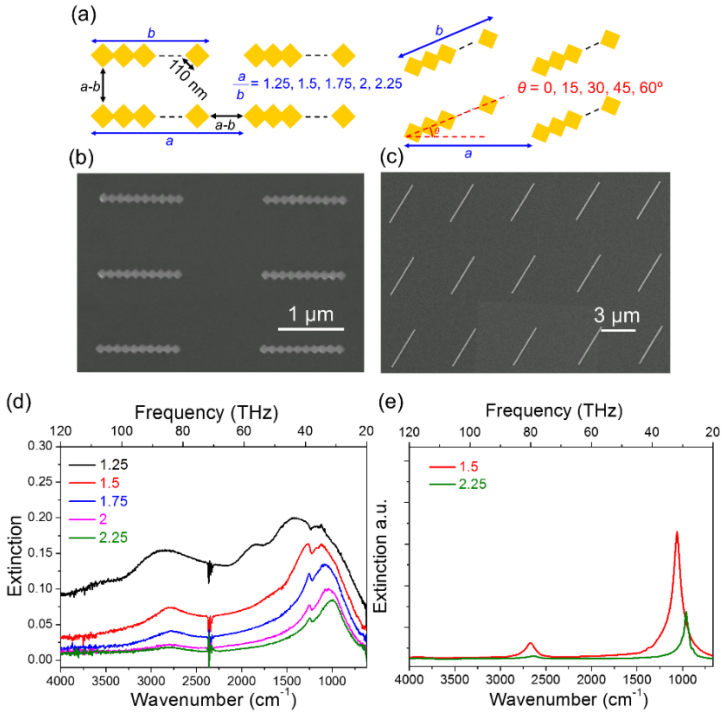

Fig. 4. (a) An ordered array of gold nanochains with square nanostructures; a/b is defined as the structural periodicity relative to the chain length, and θ is defined as a rotating angle relative to the transverse axis. SEM images of gold nanochains containing ten and thirty square nanostructures (a/b = 2) with θ of 0 (b) and 60° (c), respectively. (d) Extinction spectra of gold nanochains composed of ten square nanostructures with various structural periodicity ratios (a/b: 1.25, 1.5, 1.75, 2, and 2.25); θ was set at 0. (e) FDTD extinction spectra of gold nanochains with ten square nanoblocks (a/b: 1.5 and 2.25).

On the other hand, an additional peak of approximately 2750 cm^{-1} appeared when a/b was reduced to 1.5. Based on the FDTD simulation, the additional peak was assigned to the hexapole mode. The representative FDTD extinction spectra of gold nanochains with ten square nanostructures (a/b: 1.5 and 2.25) are shown in Fig. 4(e). Notably, the hexapole mode at approximately 2700 cm^{-1} appeared in the FDTD simulation as well when a/b had the relatively smaller value of 1.5. Thus, the FDTD extinction spectra nearly reproduced the experimental extinction spectra.

The spectral properties concerning the extinction value and the peak ratio between dipole and hexapole modes as functions of a/b and θ are summarized in Fig. 5. For all θ, the extinction value increased with decreasing a/b because the structural density increased when the structural periodicity became small. It is noteworthy that the frequency selectivity, which is highly dependent on the peak ratio between dipole and hexapole modes, is suitable for larger periodicity and an appropriate angle because the inter-structural distance becomes longer with the rotating angle. Although the extinction value and the peak ratio between dipole and hexapole modes are inversely related and thus necessitate a trade-off, there is an optimal configuration that offers a high frequency selectivity and a relatively high extinction value (e.g., a/b = 2 and θ = 60°). We performed the same experiments and analyses using gold nanochains with five and fifteen square nanostructures and found that the optimized conditions were nearly same as with ten nanostructures.

Optics EXPRESS

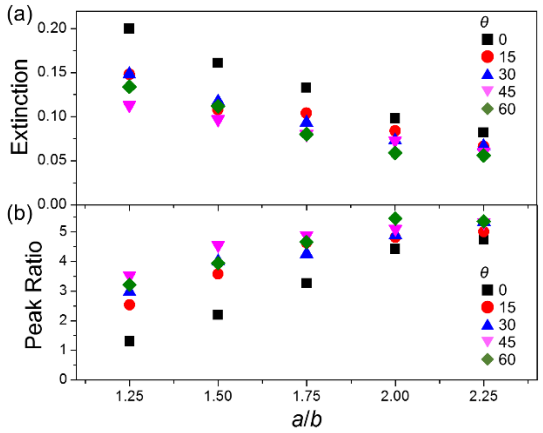

Fig. 5. (a) Plots of the extinction value at the peak wavenumber of the dipole resonance band as a function of a/b and θ; (b) Peak ratio between dipole and hexapole modes as a function of a/b.

Thus, we have fabricated long gold nanochains composed of square nanostructures with a/b of 2 and θ of 60° as shown in SEM image of Fig. 4(c). Figure 6(a) shows the extinction spectra of gold nanochains with thirty square nanostructures with the substrate as a reference. A nearly symmetric dipole resonance band can be observed in the frequency region at approximately 370 cm^{-1} (11 THz). Figure 6(b) indicates the chain length dependence of the resonant wavelength. The resonant wavelength increases linearly with increasing chain length, similar to Fig. 2(c). Therefore, we have successfully controlled plasmon resonance in the near-infrared to the far-infrared regions with a high frequency selectivity using gold nanochains with square nanostructures and the appropriate structural periodicity and arrangement to inform the design of plasmonic antennae.

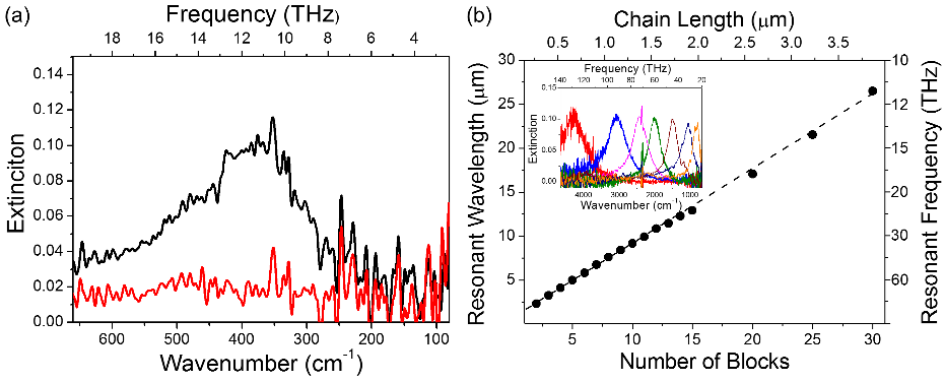

Fig. 6. (a) Extinction spectra of gold nanochains with thirty square nanostructures (black line) compared to the substrate (red line). (b) Chain length dependence of the resonant wavelength. Inset shows extinction spectra for different lengths of gold nanochain composed of square nanoblocks; two blocks red line, three blocks blue line, four blocks pink line, five blocks green line, seven blocks dark brown line, ten blocks navy line, and fourteen blocks orange line.

3.3 Improvement of resonant efficiency using ring-type gold nanochains

One of the drawbacks of gold nanochains is their low resonant efficiency because gold nanochains are sensitive only to the linear polarized light along the chain. To overcome this drawback, an isotropic antenna shape on the substrate surface is required to interact with non-polarized light efficiently. Gold disks are straightforward to design and fabricate by lithography as a representative isotropic antenna shape on the substrate surface. However, it is known that multiple plasmonic modes are excited [20]. The design of a cross-shaped gold

Optics EXPRESS

nanochain (two nanochains cross right-angled at center of chains), which can interact with non-polarized light, were also considered. However, the hexapole peak still remains although the extinction value increased about twice as compared to that of a straight nanochain from the FDTD simulation (the data were not shown here). Therefore, we designed ring-type gold nanochains as shown in the SEM images of Fig. 7(a), which shows eighteen, thirty-six, and sixty circular nanostructures (diameter: 155 nm) arranged in a circle. The thickness of each nanochain was fabricated to be 30 nm. Figure 7(b) shows extinction spectra of the ring-type gold nanochains composed of circular nanostructures with various ring diameters. The ring diameter was defined as the outer diameter. The plasmon band exhibits a lower frequency shift with increasing ring diameter. Therefore, we plotted the peak wavelength as a function of the ring diameter as shown in Fig. 7(c). The resonant wavelength linearly increases with increasing ring diameter.

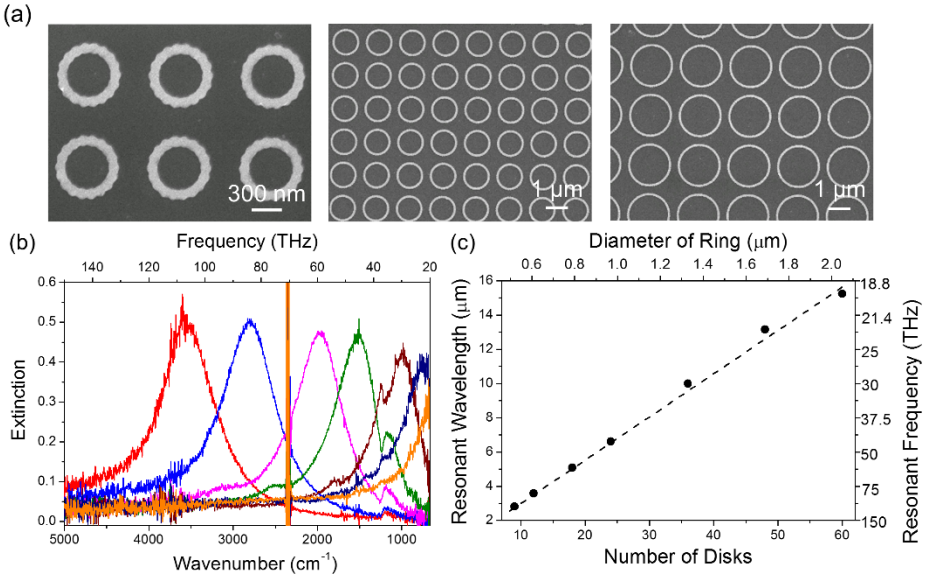

Fig. 7. (a) SEM images of god nanochains consisting of eighteen, thirty-six, and sixty circular nanostructures arranged in a circle. (b) Extinction spectra of the ring-type gold nanochains composed of circular nanostructures with different ring diameters: 0.51 μm red line, 0.61 μm blue line, 0.80 μm pink line, 0.96 μm green line, 1.35 μm dark brown line, 1.69 μm navy line, and 2.05 μm orange line. (c) Peak wavelength vs. ring diameter.

Notably, distinct higher-order plasmon resonance modes were not observed in the spectra. It can be concluded that damping was induced because of the curvature. Analogous to the straight gold nanochains with narrower bottlenecks described in 3.1, the damping induced broadening of the dipole resonance spectrum and suppression of higher-order plasmon resonances. We performed FDTD simulation using the design of the ring-type and the straight gold nanochains with circular nanostructures. Figure 8(a) shows FDTD extinction spectra of ring-type and straight gold nanochains with a diameter of 1.35 μm and a chain length of 1.35 μm, respectively. The hexapole peak is not observed in ring-type gold nanochains although that is observed in straight gold nanochains. Therefore, it was confirmed that frequency selectivity is high in the ring-type gold nanochains as well as in FDTD simulations. Figure 8(b) shows the FWHM as a function of resonant frequency. The spectral width of ring-type gold nanochains became broader than that of straight gold nanochains even with square nanostructures. However, only 20% of light was transmitted in the case of the ring-type gold nanochains, although 80% of light is transmitted without interaction in the case of the straight gold nanochains. (These values are estimated using the extinction values.) Therefore, the ring-type

Optics EXPRESS

gold nanochain is also a promising design for infrared antennae with high frequency selectivity and resonant efficiency.

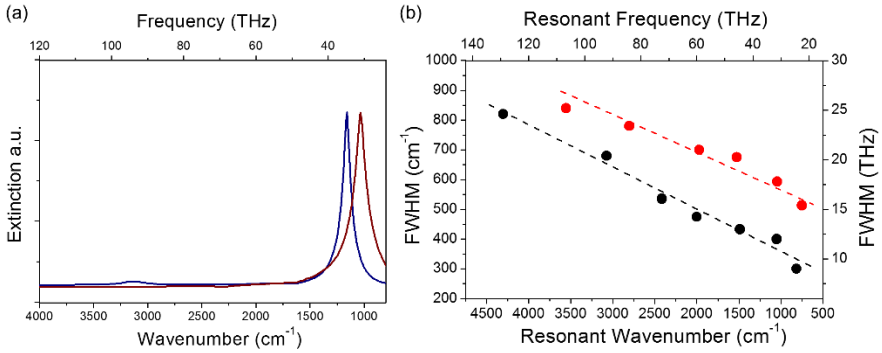

Fig. 8. (a) FDTD extinction spectra of ring-type and straight gold nanochains with a diameter of 1.35 μm (dark brown line) and chain length (navy line) of 1.35 μm, respectively. (b) The resonant wavenumber dependence of the spectral width as FWHM with ring-type (red) and straight (black) gold nanochains, respectively.

4. Conclusion

We have studied the spectral properties of gold nanochains to explore the design of optical antennae with higher resonant efficiency and frequency selectivity. The excitation of hexapole mode was suppressed because of the narrower bottleneck width of approximately 30 nm and longer inter-structural distance compared to the chain length. In particular, the gold nanochains containing square nanostructures that were used as an optical antenna enable high frequency selectivity. However, the straight gold nanochains suffer from the disadvantage that the resonant efficiency is relatively low because gold nanochains are sensitive only to linear polarized light along the chain. The ring-type gold nanochains containing circular nanostructures arranged in a circle are found to be a promising configuration for optical antennae in the infrared region, as they exhibit a high resonant frequency and relatively high frequency selectivity. These antenna designs can be customized according to the specific application. This study provides guidelines for optimizing the structural design of optical antennae in the infrared region.

Acknowledgments

We gratefully acknowledge financial support from JSPS KAKENHI Grant Numbers JP15H01073 (Photosynergetics), JP23225006, JP15K04589, JP15H00856 (AnApple), the Nanotechnology Platform (Hokkaido University), and Dynamic Alliance for Open Innovation Bridging Human, Environment and Materials (Five-Star Alliance) of MEXT.